Elongation of skyrmions by Dzyaloshinskii-Moriya interaction in helimagnetic films

Yingying Dai[1,*], Han Wang[1], Teng Yang[1], Adekunle O. Adeyeye[2,†], Zhidong Zhang[1]

[1] *Shenyang National Laboratory for Materials Science, Institute of Metal Research, Chinese Academy of Sciences, 72 Wenhua Road, Shenyang 110016, People's Republic of China*

[2]*Department of Electrical and Computer Engineering, National University of Singapore, 4 Engineering Drive 3, Singapore 117583, Singapore*

[†]*Present Address: Department of Physics, Durham University, South Road, Durham DH1 3LE, United Kingdom.*

**Email: yydai11b@imr.ac.cn*

Abstract

Distortion of skyrmions arouses much attention recently due to the exotic topological and dynamic properties. Investigating the formation mechanism and dynamical behavior of the deformed skyrmions promotes practical spintronic applications. Elongation, as a typical form of deformation, has been discovered both in experiments and in theories. However, its intrinsic mechanism is absent. Here we observe the coexistence of zero-field circular and elongated skyrmions in helimagnetic films. The elongated skyrmions, which are determined by the intrinsic Dzyaloshinskii-Moriya interaction (DMI), carry the same topological charge as the circular ones and show the skyrmion Hall effect. Current-driven dynamics reveals again the significant role of the intrinsic DMI playing in the skyrmion elongation.

Article Highlights

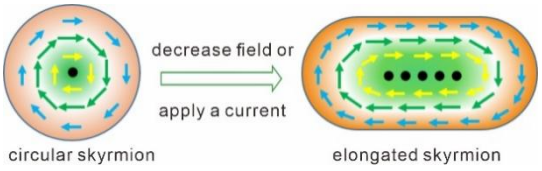

Keywords: elongated skyrmions, Dzyaloshinskii-Moriya interaction, skyrmion Hall effect, zero-field skyrmions

Introduction

Magnetic skyrmions are particle-like topologically-protected solitons, which have potential applications in future low-power magnetic storage and spintronics [1-4]. Skyrmions existing in chiral magnets are stabilized by the spin-orbit-coupling-induced Dzyaloshinskii-Moriya interaction (DMI) in non-centrosymmetric magnets [5, 6]. In these magnets with bulk DMI, skyrmions can form when an appropriate external magnetic field is applied and temperature is near the critical temperature of a magnetic transition [7, 8]. Most of the previous work were focused on the quasiparticle properties of skyrmions due to the topological protection. However, skyrmions can undergo significant deformations when driven by an external magnetic field, a current [9-12] or a magnetic-field-cooling process [13].

Recently, deformation of a single skyrmion and phase transition of a skyrmion lattice have been received gradually increasing attentions because of the exotic dynamics of distorted skyrmions [13-17]. The elongated skyrmions can be formed either by decreasing an external magnetic field at a non-equilibrium state [14], by a high current density which distorts circular skyrmions [11, 18], or by merging two or more circular skyrmions [16]. Interestingly, a circular skyrmion can be divided into two circular skyrmions by enlarging the skyrmion into an intermediate elongated skyrmion in a current with high density or in a magnetic field pulse [19, 20]. Elongated skyrmions can affect skyrmion dynamics, especially the drive-dependent skyrmion Hall angle [21, 22]. However, the elongation mechanism of skyrmions remains elusive. It is attributed by some researchers to the field-like spin-orbit torque (SOT) [22] or the damping-like SOT [21] which are aroused by current, while it can be considered also in

terms of coalescence of two or more circular skyrmions [16, 23]. But the mechanisms above are rather extrinsic, some possible intrinsic factors have not been unveiled yet. Therefore, it is of great importance to investigate the formation mechanism of the elongated skyrmions, to understand the elongation effect on skyrmion dynamics and their potential applications in high-density storage and spintronics.

In this work, we demonstrate the formation of zero-field elongated skyrmions in helimagnets. We find that the intrinsic antisymmetric exchange interaction DMI, other than current driving or skymions' coalescence, results in formation of elongated skyrmions. With increasing the DMI constant, number of skyrmions increases, while the average length of the elongated skyrmions decreases. The elongated skyrmion carries the same skyrmion winding number as the circular one and also shows the skyrmion Hall effect, which distinguishes the elongated skyrmion from stripe domains. Driven by a current, skyrmions can be changed between the circular and elongated ones. The elongated skyrmions do not go back to the circular ones when driving current is switched off, confirming the important role of the intrinsic DMI in maintaining the elongated skyrmions.

Micromagnetic Methods

The three-dimensional object oriented micromagnetic framework (OOMMF) code [24] was used to study the formation mechanism and dynamics of the elongated skyrmions in helimagnets. To simulate the effect of the spin-transfer torque due to the in-plane current, the Landau-Lifshitz-Gilbert (LLG) equation is modified as follows [25]:

$$\frac{\partial \mathbf{m}}{\partial t} = -|\gamma|\mathbf{m} \times \mathbf{H}_{eff} + \alpha \mathbf{m} \times \frac{\partial \mathbf{m}}{\partial t} + u\mathbf{m} \times \left[\mathbf{m} \times \frac{\partial \mathbf{m}}{\partial x}\right] - \beta u \mathbf{m} \times \frac{\partial \mathbf{m}}{\partial x}, \quad (1)$$

$$u = \frac{JPg\mu_B}{2eM_s}, \quad (2)$$

where $\mathbf{m}$ is the unit vector of the local magnetization, $\mathbf{H}_{\text{eff}}$ the effective magnetic field, γ the gyromagnetic ratio, α the Gilbert damping parameter, e the electron charge, J the current density, μ_B

the Bohr magneton, P the spin current polarization of the ferromagnet and g the g-factor, β the non-adiabaticity factor and M_s the saturation magnetization.

According to Ref. [26], the physical parameters for FeGe were chosen, including the saturation magnetization $M_s = 1.5 \times 10^5$ A/m, the exchange stiffness $A_{ex} = 6.8 \times 10^{-13}$ J/m, and the bulk DMI constant $D = 1.2 \times 10^{-4}$ J/m^2. The perpendicular anisotropy K was chosen from 4×10^3 to 1.4×10^4 J/m^3 in order to investigate systematically the dependence on the anisotropy of the formation of skyrmions. D was selected from 8.55×10^{-5} to 2.85×10^{-4} J/m^2 to investigate the effect of the DMI constant. The film size was 800×800 nm^2 with the thickness in the range of 2-10 nm, and the cell size was $5 \times 5 \times 2$ nm^3 which is smaller than the exchange length of 6.93 nm. The cellsize decreased to $2 \times 2 \times 1$ nm^3 or $1 \times 3 \times 2$ nm^3, in order to exclude the influence of the cellsize on the formation of elongated skyrmions. Two-dimensional periodic boundary conditions (2D PBC) [27] were used to check the reliability of the magnetic phase diagram. The out-of-plane magnetic field B was increased from zero to 300 mT to show the magnetic transition from a helix to a ferromagnetic state. To display the deformation of skyrmions, B was then decreased from 130 mT to -230 mT. The energy minimization method was used to simulate the magnetic phase diagram. To simulate the current-driven dynamics of the elongated skyrmions, the size of the sample was chosen to be $2000 \times 1000 \times 4$ nm^3 with the 2D PBC for illustrating the skyrmion Hall effect more clearly. The current density was in the range from 1×10^{10} to 1×10^{12} A/m^2, and the Gilbert damping factor α was set to be 0.02.

Results and discussion

The influence of the magnetic field on the elongated skyrmions is represented in Fig. 1. The magnetic field is applied perpendicular to the film plane. Skyrmion winding number S, as defined by the following equations [28], is used to discern different magnetic states.

$$S = \iint q dx dy\,, \tag{3}$$

$$q \equiv \frac{1}{2}\varepsilon_{\mu\gamma}\mathbf{m}\cdot\left(\partial_\mu\mathbf{m}\times\partial_\gamma\mathbf{m}\right). \tag{4}$$

$\varepsilon_{\mu\gamma}$ is the antisymmetric tensor, q is the topological density, and $\mathbf{m}$ is the unit vector of local magnetization. By micromagnetic simulations, we drew the magnetic phase diagram for elongated skyrmions by tuning the magnetic anisotropy and the film thickness, as shown in Fig. 1. The magnetic anisotropy affects the magnetic phase diagram significantly, as illustrated in Figs. 1(a) and 1(b). In Fig. 1(a), the magnetic phase diagram shows four regions: helix, mixed state (skyrmions + helix), skyrmion lattice and ferromagnetic state, which is typical for a helimagnet [7, 29]. Without an external magnetic field, the spin texture shows a helix, which is the ground state of a helimagnet. As the magnetic field increases, the magnetic state transforms gradually from a helical state to a mixed state, then a skyrmion state and finally to a ferromagnetic state. In the skyrmion region, the skyrmion density relies sensitively on the magnetic anisotropy constant. To obtain skyrmions in the present system, we calculate the required anisotropy constant as follows. According to Refs. [30] and [31], the critical DMI constant (D_c) essential for the formation of skyrmions in a film can be evaluated by the following equations:

$$D_c = \frac{4}{\pi}\sqrt{A_{ex}K} \tag{5}$$

From which, the calculated upper limit of K in this system is 1.35×10^4 J/m^3.

The dependence of the skyrmion winding number on the anisotropy constant in an infinite film is shown in Fig. 1(a). Our simulation finds no skyrmions existing in a film when K is below 4×10^3 J/m^3, so K is taken in the range of 4×10^3~ 1.4×10^4 J/m^3 to meet the condition for skyrmions. As the anisotropy constant K increases, the skyrmion winding number (S) first increases and reaches its maximum value at K~ 8×10^3 J/m^3, as shown in Fig. 1(b), and then goes down to the lowest value when K is larger than 1.2×10^4 J/m^3. The decreasing S indicates that the spin texture changes from a skyrmion

lattice to well-isolated skyrmions when K increases. The above results illustrate that an appropriate magnetic anisotropy value is required for the existence of skyrmions in the thin films, which agrees well with the previous results in Refs. [30] and [32].

As reported previously in the articles [14, 33, 34], sweeping an external magnetic field is an effective method to enlarge the skyrmion area in the field-temperature (B-T) windows. This method also works for increasing skyrmion area in the B-K and B-thickness windows, as illustrated in Figs. 1(c) and 1(f). Figure 1(c) shows the transformation of the spin texture from the skyrmion lattice state to other magnetic states as the magnetic field sweeps from 130 to -230 mT. The magnetic state changes from the skyrmion with $S < 0$ to the skyrmion with $S > 0$, and finally reaches the field-polarized ferromagnetic state. In the $S < 0$ skyrmion region, we discover the formation of elongated skyrmions without topological phase transition. The pink dashed lines show the boundary between the circular and elongated skyrmions. The previous reports revealed that sample size has significant influence on the formation of skyrmions [7, 35]. Here, we report the effect of film thickness on the magnetic phase diagrams, as shown in Figs. 1(d) and 1(f). Similar to Fig. 1(a), Fig. 1(d) also gives a typical phase diagram of a helimagnet. Meanwhile, in the skyrmion region, the skyrmion density possesses a strong thickness dependence, as can be seen from Fig. 1(e). The number of skyrmions first increases with thickness and reaches the largest value (~34) at the thickness of 4 nm. Even though the skyrmion density changes with film thickness, the skyrmions exist in a form of lattice instead of isolated in the skyrmion region for all the thickness of interest here. Worth pointing out is that, elongated skyrmions can be stable when the magnetic field is small (between -75 mT and 75 mT here) in both Fig. 1(c) and Fig. 1(f).

Structural details of the skyrmion elongation are given in Fig. 2. From Fig. 2(a) to 2(c), along with

the sweeping field decreasing from 100 mT to zero, some circular skyrmions stretches gradually to become elongated ones. The elongation length increases with the descending field, while the total number of skyrmions remains unchanged, as shown in Fig. 2(f). It indicates that the elongation of skyrmions is not from the merging of two or more skyrmions (different from Refs. [23] and [36]), but from the directional stretching of individual skyrmions. In Fig. 2(f), though S changes a little with B, the absolute value of S is almost the same as the total number of skyrmions at zero field, indicating that the elongated skyrmions carry the same value of topological charge as the circular ones [37], and thus are also protected by the topology. The topologically protected property distinguishes the elongated skyrmions from stripe domains. Deviation of S from the total number of the skyrmions at a finite B field is due to the influence of the magnetic field and the film boundary.

The elongated skyrmions can be stable at zero magnetic field and even when reversing the magnetic field up to -50 mT. Further increasing the magnetic field enlarges the skyrmion size gradually but squeezes the orange ferromagnetic area into a very narrow stripe until an appearance of the skyrmions with $S > 0$, as illustrated in Figs. 2(d) and 2(e). In addition, the highest density for the $S > 0$ skyrmions is obtained when K is around 6×10^3 J/m^3, instead of 8×10^3 J/m^3 for the $S < 0$ skyrmions, as shown in Fig. 1(c).

To unveil the physical mechanism behind the formation of the elongated skyrmion, we look into the various energy terms in our simulations. The energy terms include the exchange interaction, anisotropy, demagnetization, Zeeman and DMI energies, among which only the demagnetization and DMI energies can lead to the distorted skyrmions in the xy plane [38]. Neglecting the demagnetization energy in the simulation, we find that the elongated skyrmions are still formed, which excludes the possible contribution of the demagnetization energy. Therefore, we consider the DMI as the only

critical factor to the formation of the elongated skyrmions.

According to Ref. [39], the energy density *w* for the bulk DMI is:

$$w_{DMI} = \mathrm{D}\left(L_{zy}^{(x)} + L_{xz}^{(y)} + L_{yx}^{(z)}\right) = D\left(m_z\frac{\partial m_y}{\partial x} - m_y\frac{\partial m_z}{\partial x} + m_x\frac{\partial m_z}{\partial y} - m_z\frac{\partial m_x}{\partial y} + m_y\frac{\partial m_x}{\partial z} - m_x\frac{\partial m_y}{\partial z}\right). \quad (6)$$

The corresponding effective field is:

$$H_{DMI} = -\frac{2D}{\mu_0 M_s}\left[\left(\frac{\partial m_z}{\partial y} - \frac{\partial m_y}{\partial z}\right)\hat{x} + \left(\frac{\partial m_x}{\partial z} - \frac{\partial m_z}{\partial x}\right)\hat{y} + \left(\frac{\partial m_y}{\partial x} - \frac{\partial m_x}{\partial y}\right)\hat{z}\right]. \quad (7)$$

For an ideal skyrmion with symmetry D_n, net DMI field is usually zero within a single skyrmion. However, spins resort to a new stable state when the external magnetic field decreases, which may result in symmetry breaking of skyrmion to decrease the demagnetization energy. In this case, net DMI field in the skyrmion becomes nonzero, which induces a stretching of circular skyrmion into an elongated one.

The DMI effect on the elongation is further investigated in Fig. 3. Figures 3(a) and 3(b) illustrate the spin textures before and after the elongation, respectively. To highlight the DMI contribution, Figs. 3(c) and 3(d) reveal the distribution of the DMI field at each grid point corresponding to that in Figs. 3(a) and 3(b). Clearly, the DMI-field distribution has similar features to the magnetization distribution. The net in-plane DMI field in a single skyrmion is marked by a black arrow in Fig. 3(c), which shows both direction and relative magnitude of the DMI field. We choose the skyrmions beyond the boundary because the skyrmion elongation at the boundary is affected by the film boundary. The directions of the black arrows in Fig. 3(c) agree well with the elongation directions of skyrmions in Fig. 3(b), indicating that the elongation is guided by the DMI field. Likewise, the new DMI field in Fig. 3(d) will further determine the new elongation direction of skyrmions when the magnetic field goes below 70 mT. The results agree well with the observation of the coexistence of circular and elongated skyrmions in the experiments [13, 40, 41].

DMI affects not only elongation direction of skyrmions, but also skyrmion density and the elongation length. The critical magnetic fields for magnetic phase transitions change monotonously with the DMI constant, as shown in Fig. 4(a). In the skyrmion region, the value of the skyrmion winding number S increases sharply with increasing the DMI constant, so does the skyrmion density. As aforementioned, sweeping the magnetic field increases the area of skyrmion in the phase diagram, and this still stands for the B-D diagram, as illustrated in Fig. 4(b). When the sweeping field changes so that the state transits from the $S < 0$ skyrmion state towards the ferromagnetic state, the elongated skyrmions and the $S > 0$ skyrmion state appear. The critical field for the phase transitions, both from the elongated skyrmion to the $S > 0$ skyrmion state and from the $S > 0$ skyrmion state to the ferromagnetic state, decreases with increasing the DMI constant. In the skyrmion region for both $S < 0$ and $S > 0$, the value of skyrmion density escalates with DMI constant, which agrees well with the literature and demonstrates the strong relevance between skyrmion density and DMI constant [41].

To have a direct impression, Figures 4(d)-4(f) show the D-dependent magnetization M_z distribution at zero magnetic field. The number of skyrmions obviously goes larger with the ascending DMI constant. At zero magnetic field, various shapes of elongated skyrmions coexist with the circular ones. Besides the bar-like shape, there are some Z-like, L-like shapes. To quantify the deformation of the elongated skyrmions, Fig. 4(c) gives the field dependence of the skyrmion core area or the percentage of core area (%) in the total area. As the DMI (or D) increases, the slope of the curves (the partial derivative of area A over B field, $\frac{\partial A}{\partial B}$) decreases, indicating that the bigger DMI (or D), the slower elongation rate. However, Area (%) reaches the same value (about 50%) at zero magnetic field for all Ds. Based on this result, we calculate the average elongation length at zero field for different Ds. As shown in Fig. 4(g), the average length of the skyrmions decreases sharply with increasing D, further

substantiating the role of DMI played in the skyrmion elongation.

Now that elongated skyrmion carries the same skyrmion winding number S as circular skyrmion, we wonder whether elongated skyrmions can also show the skyrmion Hall effect [42, 43]. Current-driven dynamics of elongated skyrmions is illustrated in Fig. 5. The current flows in the $+x$ direction, while circular skyrmions and elongated skyrmions roughly move in the $-x$ direction, as shown in Fig. 5(a). To determine whether the elongated skyrmions have the skyrmion Hall effect in the elongated ones, one has to investigate whether the elongated skyrmions can move in the y direction perpendicular to the driving current [43]. Figure 5(b) represents the time dependence of the average current-driven displacement (ΔX, ΔY) of the three elongated skyrmions (square marked in Fig. 5(a)). The elongated skyrmions move linearly in the $-x$ direction with a velocity v_x of -6.698 m/s, and almost linearly in the $+y$ direction with a velocity v_y of 0.103 m/s, which indicates that the elongated skyrmions do have the skyrmion Hall effect, just like the circular ones.

Previous experimental work reported current-induced skyrmion deformation and it would go back to circular skyrmion when current is switched off [21]. To understand the role of current in this work, we study the effect of current density on the elongation. As shown in Fig. 6, first of all, when a small current density is applied, e.g., less than 1×10^{10} A/m^2, circular and elongated skyrmions move without obvious deformations, and the number of elongated skyrmions remains unchanged with time. This rules out small current as a source of skyrmion elongation. Second, when the current density goes higher than the critical value, for example in the range of 1×10^{10} ~1×10^{11} A/m^2, the number of elongated skyrmions increases monotonically from 6 to 12, with some additional skyrmions elongated and finally saturated, which indicates an irreversible current-driven elongation of circular skyrmions. The deformation of circular skyrmions driven by current is caused by the difficulty to maintaining the

spin texture of skyrmion with a large velocity [11, 18]. Finally, when the current density is larger than 1 $\times 10^{11}$ A/m^2, skyrmions can be transformed between the circular and elongated ones, therefore, the number of elongated skyrmions fluctuates with time. The fluctuation suggests that skyrmion elongation can be assisted by the field-like or damping-like torque given by the current besides the DMI [21, 22]. However, after switching off the current, the deformed skyrmions are frozen and do not shrink back to the circular skyrmions (Fig. 6(b)), which is quite distinguished from the experimental results [21]. This irreversible process indicates that the elongated skyrmions here are stabilized by the DMI, instead of by the field-like or damping-like torque given by the current. Note that, the skyrmion winding number S remains the same value when driven by the current, which rules out the possibility of new skyrmions or melting two or more skyrmions into one elongated skyrmion.

An elongated skyrmion may easily split into two skyrmions in a smaller field or at a lower current density compared to that used in the circular one, because circular skyrmion, if used for splitting, has to go through elongation in the first place which costs much energy [11, 19, 20]. Such an advantage in the already elongated skyrmion may be used to increase the skyrmion density for high-density storage applications.

Since antiferromagnet can be tuned by strain [44-46], it would be curious and interesting for us to wonder whether deformation of the antiferromagnetic (AFM) skyrmions can appear. As seen from Figs. 1 and 3, sensitivity to an external magnetic field and D_n symmetry breaking of the DMI field are the two key factors to obtain elongated skyrmions. Therefore, to obtain elongated AFM skyrmions means to search for an antiferromagnet which can meet the two conditions. However, for a collinear antiferromagnet, it holds robustness against magnetic fields making the field tuning implausible [46], and DMI field at each point due to the two magnetic sublattices of the antiferromagnet may cancel out

resulting in zero net in-plane DMI field. Thus, it is difficult to obtain elongated AFM skyrmions obtained in collinear antiferromagnet. However, it is still possible for one to have AFM skyrmions elongated in a non-collinear antiferromagnet if the D_n or C_{nv} symmetry can be broken by deceasing the external magnetic field. Besides, as indicated in Ref. [44-47], strain, which seems to a generic means to tuning not only the anomalous Hall conductivity, but also the skyrmions deformation, can probably be used for elongated AFM skyrmions.

Conclusions

We have systematically investigated the mechanism behind the skyrmion elongation in helimagnets. We observe that the elongated skyrmions arise from the deformation of the circular ones other than the merging of two or more skyrmions. The elongated skyrmions share some similar properties with the circular ones, for example, the topological charge and the skyrmion Hall effect. We find that DMI determines the elongation directions of skyrmions and stabilizes elongated skyrmions. In addition, the driving current plays some roles in changing elongation number and the elongated skyrmions do not shrink back to the circular ones when current is turned off, which rules out the effect of the field-like or damping-like torque of driving current and further supports the significant role of the intrinsic DMI in generating and stabilizing skyrmion elongation.

Acknowledgements

The work is supported by the National Natural Science Foundation of China under Grant Nos. 51701217, 51590883, 52031014.

Statements and Declarations

Conflict of interests The authors declare that they have no conflict of interest.

References

[1] Yu XZ, Onose Y, Kanazawa N, Park JH, Han JH, Matsui Y, Nagaosa N, Tokura Y. Real-space observation of a two-dimensional skyrmion crystal. Nature. 2010; 465: 901.

[2] Sampaio J, Cros V, Rohart S, Thiaville A, Fert A. Nucleation, stability and current-induced motion of isolated magnetic skyrmions in nanostructures. Nat. Nanotechnol. 2013; 8: 839.

[3] Zhang X, Ezawa M, Zhou Y. Magnetic skyrmion logic gates: conversion, duplication and merging of skyrmions. Sci. Rep. 2015; 5: 9400.

[4] Wei W-S, He Z-D, Qu Z, Du H-F. Dzyaloshinsky-Moriya interaction (DMI)-induced magnetic skyrmion materials. Rare Metals 2021; 40: 3076.

[5] Dzyaloshinsky I. A thermodynamic theory of "weak" ferromagnetism of antiferromagnetics. J. Phys. Chem. Solids. 1958; 4: 241.

[6] Moriya T. Anisotropic superexchange interaction and weak ferromagnetism. Phys. Rev. 1960; 120: 91.

[7] Yu XZ, Kanazawa N, Onose Y, Kimoto K, Zhang WZ, Ishiwata S, Matsui Y, Tokura Y. Near room-temperature formation of a skyrmion crystal in thin-films of the helimagnet FeGe. Nat. Mater. 2011; 10: 106.

[8] Mühlbauer S, Binz B, Jonietz F, Pfleiderer C, Rosch A, Neubauer A, Georgii R, Böni P. Skyrmion Lattice in a Chiral Magnet. Science. 2009; 323: 915.

[9] Dai Y, Wang H, Yang T, Ren W, Zhang Z. Flower-like dynamics of coupled Skyrmions with dual resonant modes by a single-frequency microwave magnetic field. Sci. Rep. 2014; 4: 6153.

[10] Wang H, Dai Y, Yang T, Ren W, Zhang Z. Dual-frequency microwave-driven resonant excitations of skyrmions in nanoscale magnets. RSC Adv. 2014; 4: 62179.

[11] Litzius K, Leliaert J, Bassirian P, Rodrigues D, Kromin S, Lemesh I, Zazvorka J, Lee K-J, Mulkers J, Kerber N, Heinze D, Keil N, Reeve RM, Weigand M, Van Waeyenberge B, Schütz G, Everschor-Sitte K, Beach GSD, Kläui M. The role of temperature and drive current in skyrmion dynamics. Nat. Electron. 2020; 3: 30.

[12] Dai YY, Wang H, Tao P, Yang T, Ren WJ, Zhang ZD. Skyrmion ground state and gyration of skyrmions in magnetic nanodisks without the Dzyaloshinsky-Moriya interaction. Phys. Rev. B 2013; 88: 054403.

[13] Morikawa D, Yu X, Karube K, Tokunaga Y, Taguchi Y, Arima T-h, Tokura Y. Deformation of Topologically-Protected Supercooled Skyrmions in a Thin Plate of Chiral Magnet $Co_8Zn_8Mn_4$. Nano Lett. 2017; 17: 1637.

[14] Yu X, Morikawa D, Yokouchi T, Shibata K, Kanazawa N, Kagawa F, Arima T-H, Tokura Y. Aggregation and collapse dynamics of skyrmions in a non-equilibrium state. Nat. Phys. 2018; 14: 832.

[15] Huang P, Schönenberger T, Cantoni M, Heinen L, Magrez A, Rosch A, Carbone F, Rønnow HM. Melting of a skyrmion lattice to a skyrmion liquid via a hexatic phase. Nat. Nanotechnol. 2020; 15: 761.

[16] Rendell-Bhatti F, Lamb RJ, van der Jagt JW, Paterson GW, Swagten HJM, McGrouther D. Spontaneous creation and annihilation dynamics and strain-limited stability of magnetic skyrmions. Nat. Commun. 2020; 11: 3536.

[17] Jena J, Göbel B, Ma T, Kumar V, Saha R, Mertig I, Felser C, Parkin SSP. Elliptical Bloch skyrmion chiral twins in an antiskyrmion system. Nat. Commun. 2020; 11: 1115.

[18] Masell J, Rodrigues DR, McKeever BF, Everschor-Sitte K. Spin-transfer torque driven motion, deformation, and instabilities of magnetic skyrmions at high currents. Phys. Rev. B 2020; 101:

214428.

[19] Müller GP, Bessarab PF, Vlasov SM, Lux F, Kiselev NS, Blügel S, Uzdin VM, Jónsson H. Duplication, Collapse, and Escape of Magnetic Skyrmions Revealed Using a Systematic Saddle Point Search Method. Phys. Rev. Lett. 2018; 121: 197202.

[20] Koshibae W, Nagaosa N. Theory of current-driven skyrmions in disordered magnets. Sci. Rep. 2018; 8: 6328.

[21] Juge R, Je S-G, Chaves DdS, Buda-Prejbeanu LD, Peña-Garcia J, Nath J, Miron IM, Rana KG, Aballe L, Foerster M, Genuzio F, Menteş TO, Locatelli A, Maccherozzi F, Dhesi SS, Belmeguenai M, Roussigné Y, Auffret S, Pizzini S, Gaudin G, Vogel J, Boulle O. Current-Driven Skyrmion Dynamics and Drive-Dependent Skyrmion Hall Effect in an Ultrathin Film. Phys. Rev. Applied 2019; 12: 044007.

[22] Litzius K, Lemesh I, Krüger B, Bassirian P, Caretta L, Richter K, Büttner F, Sato K, Tretiakov OA, Förster J, Reeve RM, Weigand M, Bykova I, Stoll H, Schütz G, Beach GSD, Kläui M. Skyrmion Hall effect revealed by direct time-resolved X-ray microscopy. Nat. Phys. 2016; 13: 170.

[23] Wild J, Meier TNG, Pöllath S, Kronseder M, Bauer A, Chacon A, Halder M, Schowalter M, Rosenauer A, Zweck J, Müller J, Rosch A, Pfleiderer C, Back CH. Entropy-limited topological protection of skyrmions. Sci. Adv. 2017; 3: e1701704.

[24] Donahue MJ, Porter DG, OOMMF User's Guide, Version 2.0a2, available at: *http://math.nist.gov/oommf.*

[25] Zhang S, Li Z. Roles of Nonequilibrium Conduction Electrons on the Magnetization Dynamics of Ferromagnets. Phys. Rev. Lett. 2004; 93: 127204.

[26] Turgut E, Park A, Nguyen K, Moehle A, Muller DA, Fuchs GD. Chiral magnetic excitations in FeGe films. Phys. Rev. B 2017; 95: 134416.

[27] Wang W, Mu C, Zhang B, Liu Q, Wang J, Xue D. Two-dimensional periodic boundary conditions for demagnetization interactions in micromagnetics. Comput. Mater. Sci. 2010; 49: 84.

[28] Heinze S, von Bergmann K, Menzel M, Brede J, Kubetzka A, Wiesendanger R, Bihlmayer G, Bluegel S. Spontaneous atomic-scale magnetic skyrmion lattice in two dimensions. Nat. Phys. 2011; 7: 713.

[29] Zhao X, Jin C, Wang C, Du H, Zang J, Tian M, Che R, Zhang Y. Direct imaging of magnetic field-driven transitions of skyrmion cluster states in FeGe nanodisks. Proc. Natl. Acad. Sci. U.S.A. 2016; 113: 4918.

[30] Yamada K, Hozumi S, Nakatani Y. Examination of the stability of skyrmion structures in perpendicularly-magnetized Co/Ni films. Jpn. J. Appli. Phys. 2017; 56: 050309.

[31] Guslienko KY. Néel skyrmion stability in ultrathin circular magnetic nanodots. Appli. Phys. Express. 2018; 11: 063007.

[32] Yu G, Upadhyaya P, Li X, Li W, Kim SK, Fan Y, Wong KL, Tserkovnyak Y, Amiri PK, Wang KL. Room-Temperature Creation and Spin–Orbit Torque Manipulation of Skyrmions in Thin Films with Engineered Asymmetry. Nano Lett. 2016; 16: 1981.

[33] Gallagher JC, Meng KY, Brangham JT, Wang HL, Esser BD, McComb DW, Yang FY. Robust Zero-Field Skyrmion Formation in FeGe Epitaxial Thin Films. Phys. Rev. Lett. 2017; 118: 027201.

[34] Oike H, Kikkawa A, Kanazawa N, Taguchi Y, Kawasaki M, Tokura Y, Kagawa F. Interplay between topological and thermodynamic stability in a metastable magnetic skyrmion lattice. Nat. Phys. 2016; 12: 62.

[35] Du H, Che R, Kong L, Zhao X, Jin C, Wang C, Yang J, Ning W, Li R, Jin C, Chen X, Zang J, Zhang Y, Tian M. Edge-mediated skyrmion chain and its collective dynamics in a confined geometry. Nat. Commun. 2015; 6: 8504.

[36] Milde P, Köehler D, Seidel J, Eng LM, Bauer A, Chacon A, Kindervater J, Müehlbauer S, Pfleiderer C, Buhrandt S, Schüette C, Rosch A. Unwinding of a Skyrmion Lattice by Magnetic Monopoles. Science 2013; 340: 1076.

[37] Ezawa M. Compact merons and skyrmions in thin chiral magnetic films. Phys. Rev. B 2011; 83: 100408(R).

[38] Beg M, Carey R, Wang W, Cortés-Ortuño D, Vousden M, Bisotti MA, Albert M, Chernyshenko D, Hovorka O, Stamps RL, Fangohr H. Ground state search, hysteretic behaviour, and reversal mechanism of skyrmionic textures in confined helimagnetic nanostructures. Sci. Rep. 2015; 5: 17137.

[39] Cortés-Ortuño D, Beg M, Nehruji V, Breth L, Pepper R, Kluyver T, Downing G, Hesjedal T, Hatton P, Lancaster T, Hertel R, Hovorka O, Fangohr H. Proposal for a micromagnetic standard problem for materials with Dzyaloshinskii–Moriya interaction. New Journal of Physics 2018; 20: 113015.

[40] Jiang W, Upadhyaya P, Zhang W, Yu G, Jungfleisch MB, Fradin FY, Pearson JE, Tserkovnyak Y, Wang KL, Heinonen O, te Velthuis SGE, Hoffmann A. Blowing magnetic skyrmion bubbles. Science. 2015; 349: 283.

[41] Yu G, Upadhyaya P, Shao Q, Wu H, Yin G, Li X, He C, Jiang W, Han X, Amiri PK, Wang KL. Room-Temperature Skyrmion Shift Device for Memory Application. Nano Lett. 2017; 17: 261.

[42] Nagaosa N, Tokura Y. Topological properties and dynamics of magnetic skyrmions. Nat. Nanotechnol. 2013; 8: 899.

[43] Jiang W, Zhang X, Yu G, Zhang W, Wang X, Benjamin Jungfleisch M, Pearson JE, Cheng X, Heinonen O, Wang KL, Zhou Y, Hoffmann A, te Velthuis SGE. Direct observation of the skyrmion Hall effect. Nat. Phys. 2017; 13: 162.

[44] Liu ZQ, Chen H, Wang JM, Liu JH, Wang K, Feng ZX, Yan H, Wang XR, Jiang CB, Coey JMD, MacDonald AH. Electrical switching of the topological anomalous Hall effect in a non-collinear antiferromagnet above room temperature. Nat. Electron. 2018; 1: 172.

[45] Liu ZQ, Feng ZX, Yan H, Wang XN, Zhou XR, Qin PX, Guo HX, Yu RH, Jiang CB. Antiferromagnetic Piezospintronics. Adv. Electron. Mater. 2019; 5: 1900176.

[46] Yan H, Feng ZX, Shang SL, Wang XN, Hu ZX, Wang JH, Zhu ZW, Wang H, Chen ZH, Hua H, Lu WK, Wang JM, Qin PX, Guo HX, Zhou XR, Leng ZGG, Liu ZK, Jiang CB, Coey M, Liu ZQ. A piezoelectric, strain-controlled antiferromagnetic memory insensitive to magnetic fields. Nat. Nanotechnol. 2019; 14: 131.

[47] Shibata K, Iwasaki J, Kanazawa N, Aizawa S, Tanigaki T, Shirai M, Nakajima T, Kubota M, Kawasaki M, Park HS, Shindo D, Nagaosa N, Tokura Y. Large anisotropic deformation of skyrmions in strained crystal. Nat. Nanotechnol. 2015; 10: 589.

Figure Captions:

Fig. 1 Magnetic phase diagram. (a, c) Skyrmion winding number S vs. magnetic field and anisotropy constant and (d, f) S vs. magnetic field and film thickness. The sweeping magnetic field B increases from 0 to 300 mT for (a) and (d), while B decreases from 130 mT (skyrmion lattice region) via 0 mT to -230 mT for (c) and (f). Dotted Lines represent phase boundaries in (a, c, b, d), and pink dashed lines show the boundaries between circular and elongated skyrmions. The anisotropy-constant dependence and thickness dependence of the maximum number of skyrmions in (b) and (e) are extracted from the skyrmion region of the magnetic phase diagrams (a) and (d), respectively.

Fig. 2 Elongation of skyrmions. (a-e) Transformation of skyrmions from the circular ($S < 0$) to the elongated and back to the circular ones ($S > 0$) when sweeping magnetic field from 100 mT via 0 to -100 mT. (f) Field dependence of the skyrmion winding number S and the total number of skyrmions when sweeping magnetic field from 130 mT to zero.

Fig. 3 (a, b) The magnetization distribution of helimagnetic film in different magnetic fields. (c) and (d) are the corresponding DMI-field distribution to (a) and (b), respectively. The color bar shows the z component of magnetization and the DMI field. Black arrows in (c) show the in-plane direction and the relative magnitude of the net DMI field in one skyrmion.

Fig. 4 Skyrmion elongation and DMI. (a,b) Magnetic phase diagram of magnetic field vs. DMI (or D) constant. The magnetic field increases from 0 to 600 mT for (a), while decreases from 330 mT to -570 mT for (b). Dotted lines represent the phase boundaries, and pink dashed lines show the boundaries between circular and elongated skyrmions. (c) The external field dependence of the percentage of the skyrmion core (Area%) for different Ds. (d-f) The magnetization distribution at zero magnetic field for different Ds when decreasing field from $S < 0$ skyrmion state. The inset in (f) shows the zoom-in image of the magnetization distribution at the right-upper corner of (f). (g) The D dependence of the average length of skyrmions at zero field.

Fig. 5 Current-driven skyrmion dynamics in the perpendicular field of 78 mT. The current density applied along the $+x$ direction is 5×10^{11} A/m^2. Two-dimensional periodic boundary conditions are used here. (a) Magnetization distribution at different time. (b)Time dependence of the average displacement (ΔX, ΔY) of the three elongated skyrmions marked in (a). Black (ΔX) and red dots (ΔY) represent the averaged center positions. The linear fits of the data are labeled by the black lines.

Fig. 6 (a) Time dependence of number of elongated skyrmions driven by in-plane current under different current densities. The out-of-plane magnetic field is 78 mT. (b) The magnetization distribution at the initial time (0 ns) when current is switched on, at 7500 ns, and at 100 ns after current is switched off. The current density is 5×10^{11} A/m^2.

Figures:

Fig.1

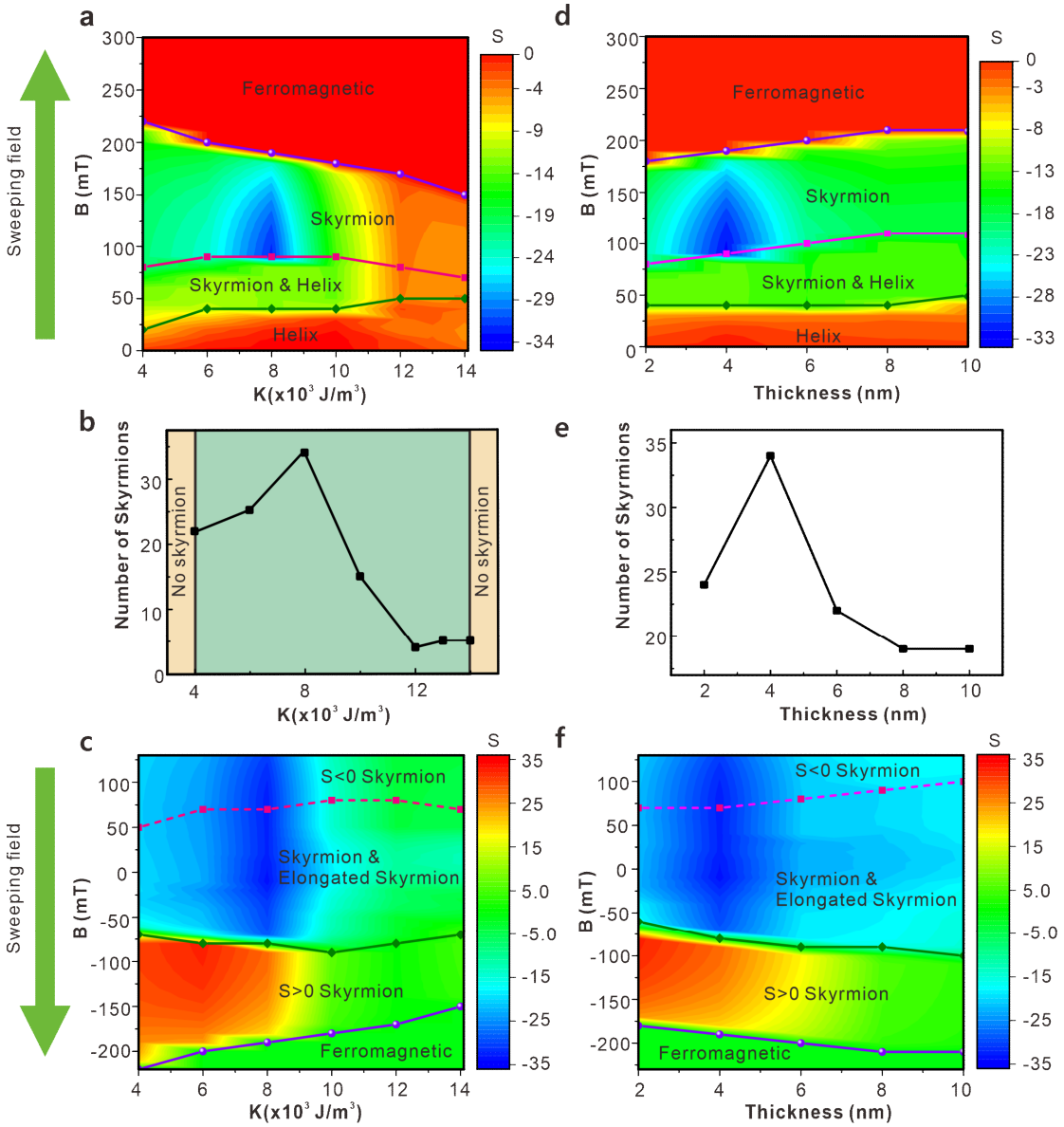

Fig. 2

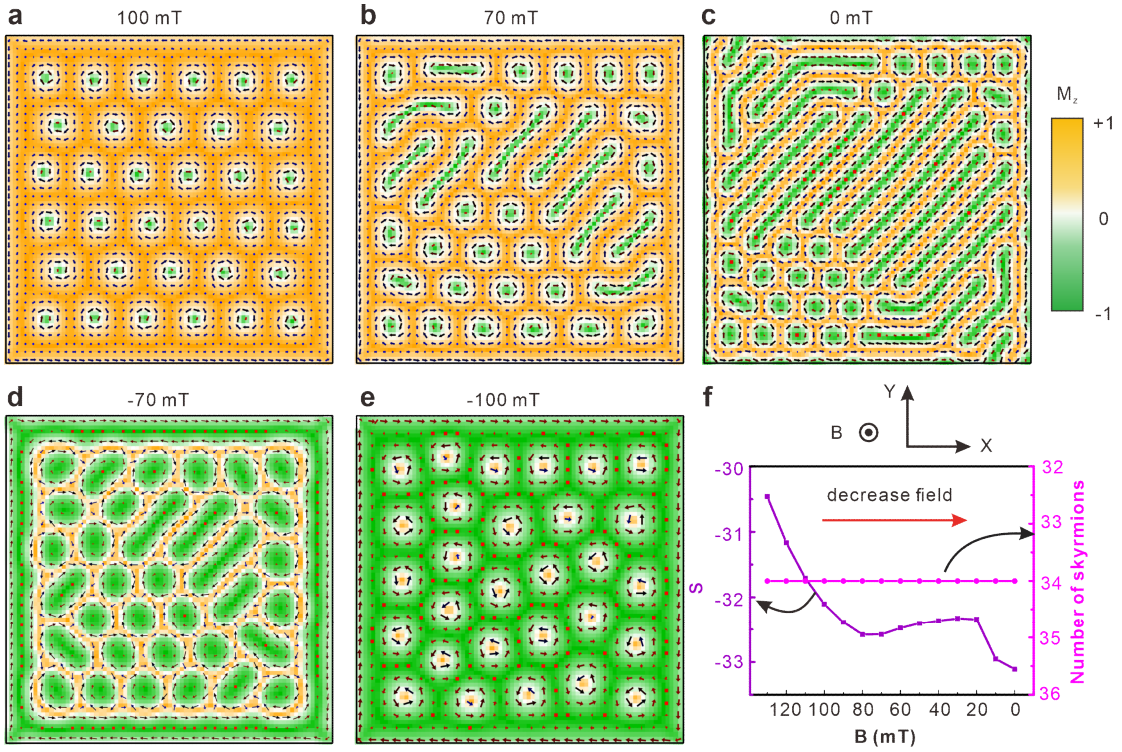
a
100 mT
b
70 mT
c
0 mT
M_z
+1
0
-1
d
-70 mT
e
-100 mT
f
B
Y
X
decrease field
S
-30
-31
-32
-33
32
33
34
35
36
Number of skyrmions
120 100 80 60 40 20 0
B (mT)

Fig. 3

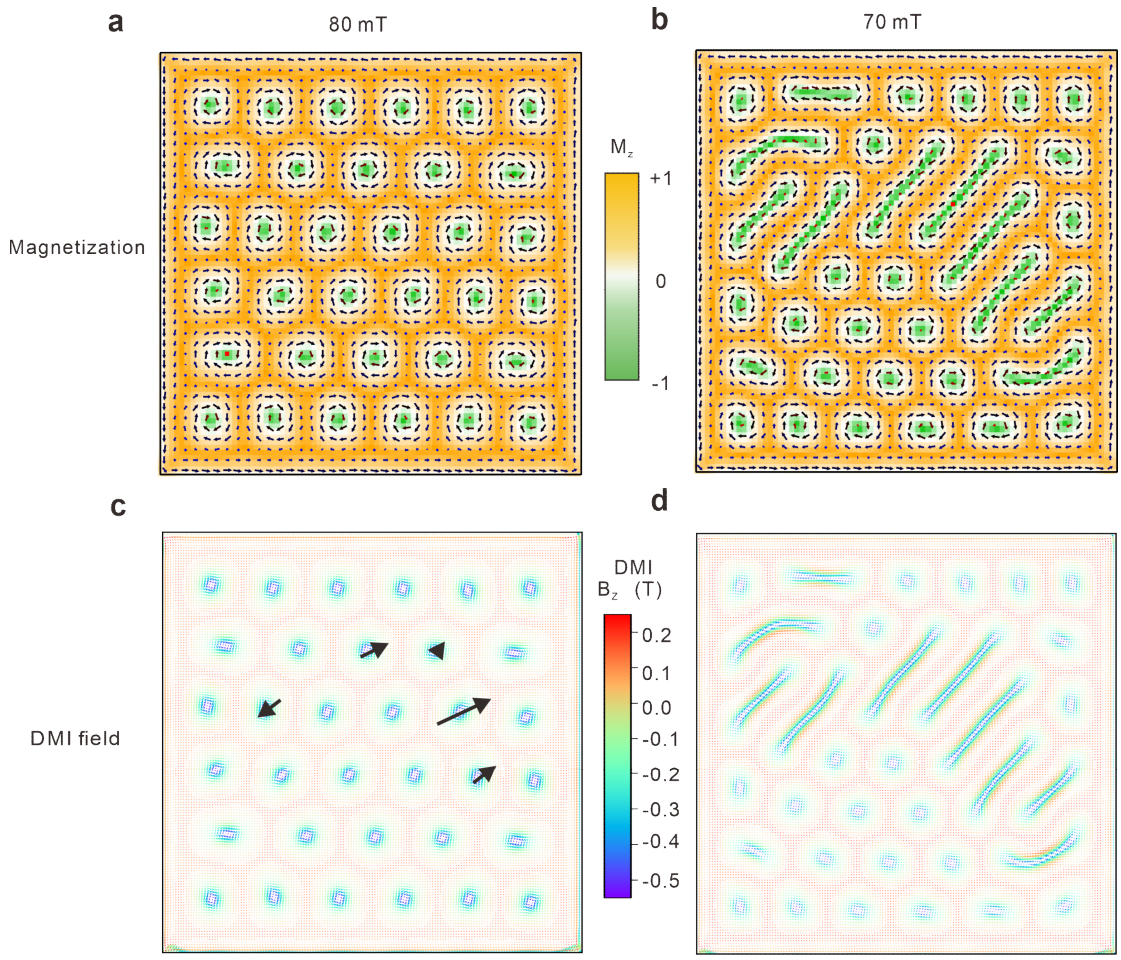
a
80 mT
b
70 mT
Magnetization
M_z
+1
0
-1
c
d
DMI field
DMI
B_z (T)
0.2
0.1
0.0
-0.1
-0.2
-0.3
-0.4
-0.5

Fig. 4

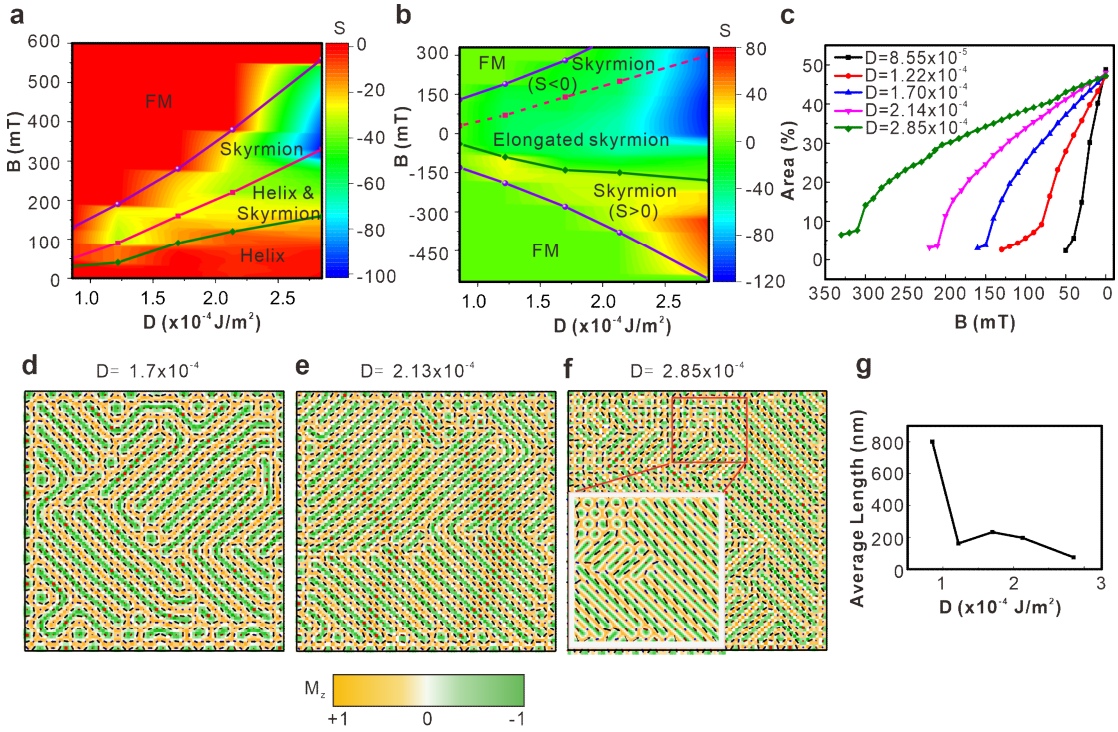
a
b
c
FM
Skyrmion
Helix & Skyrmion
Helix
Elongated skyrmion
Skyrmion (S<0)
Skyrmion (S>0)
B (mT)
D (x10⁻⁴ J/m²)
S
Area (%)
B (mT)
D=8.55x10⁻⁵
D=1.22x10⁻⁴
D=1.70x10⁻⁴
D=2.14x10⁻⁴
D=2.85x10⁻⁴
d
D= 1.7x10⁻⁴
e
D= 2.13x10⁻⁴
f
D= 2.85x10⁻⁴
g
Average Length (nm)
D (x10⁻⁴ J/m²)
Mz
+1
0
-1

Fig. 5

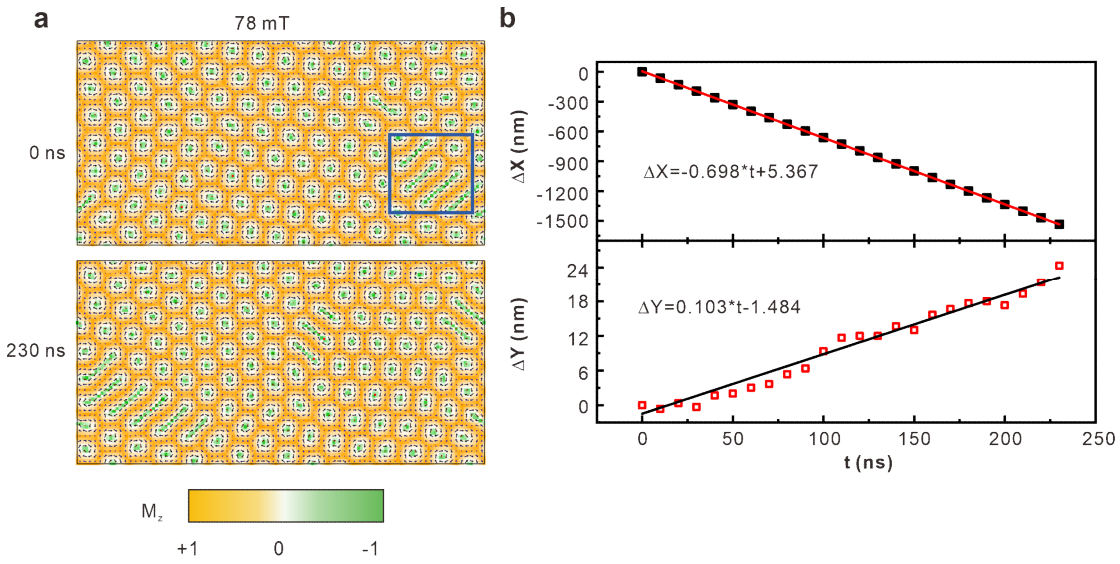
a
78 mT
0 ns
230 ns
M_z
+1
0
-1
b
ΔX (nm)
ΔX=-0.698*t+5.367
ΔY (nm)
ΔY=0.103*t-1.484
t (ns)

Fig. 6

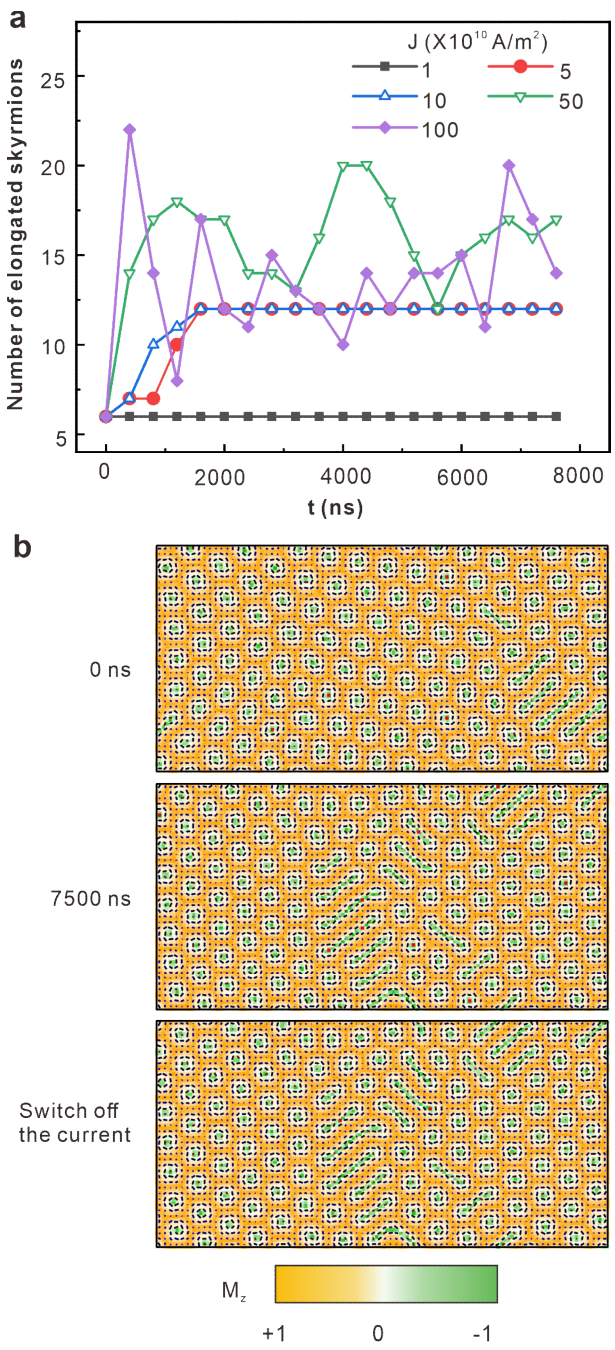
a
Number of elongated skyrmions
t (ns)
J (X10^10 A/m^2)
1
5
10
50
100
b
0 ns
7500 ns
Switch off
the current
M_z
+1
0
-1